Biochimica et Biophysica Acta 1848 (2015) 2967–2979

Contents lists available at ScienceDirect

Biochimica et Biophysica Acta

journal homepage: www.elsevier.com/locate/bbamem

Charge and aggregation pattern govern the interaction of plasticins with LPS monolayers mimicking the external leaflet of the outer membrane of Gram-negative bacteria

J.P. Michel [a,b,*], Y.X. Wang [a,b], E. Dé [c,d], P. Fontaine [e], M. Goldmann [e,f,g], V. Rosilio [a,b]

[a] Univ Paris-Sud, Institut Galien Paris Sud, 5 rue Jean-Baptiste Clément, F-92296 Châtenay-Malabry cedex, France
[b] CNRS, UMR 8612, F-92296 Châtenay-Malabry, France
[c] Normandie Univ, France
[d] CNRS, UMR 6270, F-76821 Mont-Saint-Aignan Cedex, France
[e] Synchrotron SOLEIL, L'Orme des Merisiers, Saint Aubin, BP48, F-91192 Gif-sur-Yvette Cedex, France
[f] INSP, UPMC, 5 place Jussieu, F-75005 Paris, France
[g] CNRS, UMR 7588, F-75005 Paris, France

ARTICLE INFO

Article history:
Received 15 April 2015
Received in revised form 1 September 2015
Accepted 2 September 2015
Available online 4 September 2015

Keywords:
Gram-negative bacteria
Monolayer
Liposome
Lipopolysaccharide
Plasticin
Grazing incidence X-ray diffraction, Atomic force microscopy

ABSTRACT

Bacterial resistance to antibiotics has become today a major public health issue. In the development of new anti-infectious therapies, antimicrobial peptides appear as promising candidates. However, their mechanisms of action against bacterial membranes are still poorly understood. We describe for the first time the interaction and penetration of plasticins into lipid monolayers and bilayers modeling the two leaflets of the asymmetrical outer membrane of Gram-negative bacteria. The lipid composition of these monolayers mimics that of each leaflet: mixtures of LPS Re 595 mutant and wild type S-form from *Salmonella enterica* for the external leaflet, and SOPE/SOPG/cardiolipin (80/15/5) for the inner one. The analysis of the interfacial behavior of native (PTCDA1) and modified (PTCDA1-KF) antimicrobial plasticins showed that PTCDA1-KF exhibited better surface properties than its unmodified counterpart. Both peptides could penetrate into the model monolayers at concentrations higher than 0.1 μM. The penetration was particularly enhanced for PTCDA1-KF into the mixed LPS monolayer, due to attractive electrostatic interactions. Grazing X-ray diffraction and atomic force microscopy studies revealed the changes in LPS monolayers organization upon peptide insertion. The interaction of plasticins with liposomes was also monitored by light scattering and circular dichroism techniques. Only the cationic plasticin achieved full disaggregation and structuration in α helices, whereas the native one remained aggregated and unstructured. The main steps of the penetration mechanism of the two plasticins into lipid models of the external leaflet of the outer membrane of Gram-negative bacteria have been established.

1. Introduction

For many decades, the development of antibiotics has revolutionized the treatment of infectious diseases, saving millions of people from death. However, only 70 years after their introduction, emerging and increasing resistance to antibiotics has become a threat to public health in developed countries. One main reason responsible for this resurgence is the excessive use of broad-spectrum antibiotics, exposing a large number of bacteria to many different classes of drugs. Incorrect diagnoses followed by inadequate antibiotic therapy have contributed to accelerate bacterial resistance spreading [1].

This issue has increased the need for the discovery of new classes of antibiotic molecules, as well as for the use of original sources such as native antimicrobial peptides. The ODA (antimicrobial peptide database) has listed 1459 antimicrobial peptides including a majority of antibacterial agents [2]. Antimicrobial peptides significantly affect the integrity of the whole bacterial membrane via interaction with membrane lipids and peptidoglycan layers, although the exact mechanism has not been elucidated yet. In fact more than one mechanism seem to operate, and they all might depend upon the chemical structure of the peptide and its conformation changes following contact with a bacterial membrane [3]. A better understanding of peptide mechanism of action would open the door to the selection and development of new therapeutically active peptides.

Abbreviations: OM, outer membrane; PLs, phospholipids; LPS, lipopolysaccharide; S-LPS, smooth strain lipopolysaccharide; SOPE, 1-stearoyl-2-oleoyl-sn-glycero-3-phosphoethanolamine; SOPG, 1-stearoyl-2-oleoyl-sn-glycero-3-phospho-(1′-rac-glycerol); CL, 1′,3′-bis[1.2-dioleoyl-sn-glycero-3-phospho]-sn-glycerol; LE, liquid expanded state; LC, liquid condensed state; Kdo, 3-deoxy-D-manno-2-octulosonic acid; PMB, polymyxin B; PDI, polydispersity index; AFM, atomic force microscopy; CD, circular dichroism; BAM, Brewster angle microscopy; DLS, dynamic light scattering; GIXD, grazing incidence X-ray diffraction; FWHM, full-width at half maximum

* Corresponding author.
E-mail address: jean-philippe.michel@u-psud.fr (J.P. Michel).

http://dx.doi.org/10.1016/j.bbamem.2015.09.005
0005-2736/

South American hylid frogs synthesize in their skin numerous antimicrobial peptides belonging to the dermaseptin superfamily that protect them against microorganisms [4,5]. These peptides are derived from precursors displaying a highly conserved N-terminal preprosequence and markedly varied carboxy-terminal domains. This results in a series of antimicrobial peptides with various lengths, charges, conformations and antimicrobial activities [6]. Among them, plasticins are linear peptides composed of L-amino acids, rich in Gly and Leu residues with regular, repeated 5-mer motifs GXXXG, where X is any amino acid [7]. Two 23 amino acid-long plasticins, belonging to the dermaseptin family [8] have been tested against various strains of Gram-negative and Gram-positive bacteria [9]. The native one, PTCDA1, is broadly neutral at physiological pH (−0.02) with almost no antimicrobial activity. A derivative of this plasticin has been synthesized with replacement of three residues in the sequence. The resulting peptide, PTCDA1-KF, is cationic (+2) with very good antimicrobial activity [9]. Its minimal concentration required for inhibiting Gram-negative bacteria growth ranges between 1 and 50 μM and particularly between 3 and 6 μM for *Salmonella* species [10].

Earlier works have attempted to better understand the mechanism of action of PTCDA1 and PTCDA1-KF against antimicrobial membranes by focusing on the changes in secondary structures of the two plasticins in the presence of phospholipid vesicles [11] or monolayers [12]. Combination of circular dichroism (CD) and Fourier Transform Infrared Spectroscopy indicated that the neutral and cationic plasticins were in a disordered state in phosphate buffer and adopted α-helical structures in the presence of phospholipid vesicles. PTCDA1-KF appeared mainly structured in α-helices lying flat beneath a lipid monolayer.

In contact with Gram-negative bacteria, a peptide has to cross the asymmetric outer membrane (OM) in which the two leaflets possess different lipid compositions: the external one is made of lipopolysaccharide (LPS) molecules, whereas the inner one contains a ternary mixture of phospholipids (PLs). Most of these lipids bear anionic charges. The charge of a membrane model is an important parameter because the preferred conformations of peptides upon interaction with anionic lipids seem to be α-helices [3,13]. There were many attempts to model the interaction of antimicrobial peptides with a membrane using simple models such as one or two-component monolayers or bilayers. For example, Corvis et al. showed that griseofulvin did not easily penetrate through the polar head group region of a lipid film, especially zwitterionic DMPE monolayers. However, nonpolar interactions were thought to be responsible for the persistence of the antibiotic into the phospholipid monolayers after adsorption [14]. Using the same approach, Clausell et al. [15] demonstrated that binding and insertion of polymyxin B (PMB) and its analogs into pure mutant LPS Re 595 and POPG monolayers were driven by both electrostatic and hydrophobic interactions. Also, Gidalevitz et al. analyzed the effect of the antimicrobial cationic peptide protegrin 1 on the in and out-of-plane structures of DPPC, DPPG and lipid A monolayers by X-ray diffraction measurements [16,17]. Mixtures of a zwitterionic phospholipid (such as phosphatidylethanolamine or phosphatidylcholine) and a charged one like phosphatidylglycerol were described as models taking better account of the anionic character of bacterial membranes [13,15,18,19]. However, all these models seem still far from the actual lipid composition of the two leaflets of a bacterial OM.

In the present work, we have built LPS monolayers and bilayers mimicking separately the two leaflets of *Salmonella enterica* OM, using a mixture of smooth LPS and mutant LPS Re 595 for the outer one, and a ternary mixture of phospholipids SOPE, SOPG and CL in a 80:15:5 M ratio, to mimic the PL composition of the inner one [20]. We chose hybrid phospholipids containing one saturated stearic acid (18:0) in the sn-1 position and one monounsaturated oleic acid (18:1) in order to mimic the most representative head groups, chain lengths, and unsaturation of natural lipids present in Gram-negative outer membranes [20,21]. The interaction of biomimetic LPS monolayers with peptides was analyzed by combination of surface pressure measurements, Brewster angle microscopy, grazing incidence X-ray diffraction experiments using synchrotron radiation and atomic force microscopy. Liposomes were used to assess the changes in physical properties of plasticins by dynamic light scattering and circular dichroism. We focused on the influence of the peptide charge, concentration, conformation and aggregation state in solution, its interfacial properties, as well as the composition of the model membrane, on the plasticins penetration mechanism.

2. Material and methods

2.1. Material

The two linear 23 amino acid long homologous plasticins were synthesized at the Plateforme d'Ingénierie des Protéines et Synthèse Peptidique (Ch. Piesse, IFR 83, Université Pierre et Marie Curie, Paris, France) [12]. The native plasticin PTCDA1 (GVVTDLLNTAGG LLGNLVGSLSGNH$_2$, Mw = 2125 g/mol) is broadly neutral at physiological pH. Its synthetic derivative, [^{8,12}K, ^{18}F]-Plasticine-DA1, (GVVTDLL**K**TAG**K**LLGNL**F**GSLSGNH$_2$, Mw = 2260 g/mol), abbreviated PTCDA1-KF, differs from PTCDA1 by the replacement of: (i) one asparagine and one glycine at positions 8 and 12 by two lysines, and (ii) a valine residue by a phenylalanine at position 18 [6]. Polymyxin B sulfate was purchased from Sigma-Aldrich (Saint Louis, MO). The three phospholipids 1-stearoyl-2-oleoyl-sn-glycero-3-phosphoethanolamine (SOPE, Mw = 746.05 g/mol), 1-stearoyl-2-oleoyl-sn-glycero-3-phospho-(1′-rac-glycerol) (sodium salt) (SOPG, Mw = 799.05 g/mol), and 1′.3′-bis [1.2-dioleoyl-sn-glycero-3-phospho]-sn-glycerol (sodium salt) (CL, Mw = 1501.98 g/mol) were purchased from Avanti Polar Lipids (Alabaster, AL). They were 99% pure and were used without further purification. Native smooth (source strain ATCC 9700) and mutant Re 595 (source strain 49284, Mw = 2500 g/mol) lipopolysaccharides from *S. enterica* serotype Minnesota were obtained from Sigma-Aldrich (Saint Louis, MO). Chloroform and methanol (99% pure) were analytical grade reagents from Merck (Germany). Sodium chloride, sodium phosphate monobasic monohydrate, and sodium phosphate dibasic heptahydrate were purchased from Sigma-Aldrich and their purity was higher than 98%. The buffer was a phosphate-buffered saline (PBS) solution with 100 mM sodium phosphate and 150 mM NaCl at pH 7. Ultrapure water (γ = 72.2 mN/m at 22 °C, resistivity 18.2 MΩ·cm) was produced by a Millipore Synergy 185 apparatus, coupled with a RiOs5. Prior to experiments, all glassware was soaked for an hour in a freshly prepared hot TFD4 (Franklab, Guyancourt, France) detergent solution (15% v/v), and then thoroughly rinsed with ultrapure water.

2.2. Methods

2.2.1. Assessment of peptide adsorption by surface tension measurements

Peptide adsorption at the free air/buffer interface was assessed from surface tension measurements by the Wilhelmy plate method, using a thermostated automatic digital tensiometer (K10 model from Krüss, Germany). Aliquots of peptide solutions were injected into the buffer subphase through the side arm of the measurement cell by means of a Hamilton syringe. The final concentration of the peptides in the subphase ranged from 0 up to 1 mM. The surface tension γ was recorded continuously as a function of time until equilibrium was reached. In order to maintain a constant level of liquid and avoid any drift in the measured surface tensions, all experiments were performed at 22 °C under saturated vapor pressure. Each measurement was performed at least twice. The experimental uncertainty was estimated to be 0.2 mN/m. Results were presented as the surface pressure at equilibrium π_{eq} equal to $\gamma_{buffer} - \gamma_{eq}$ versus plasticin concentration C, with γ_{buffer} the surface tension of the free air/buffer interface and γ_{eq} the surface tension at equilibrium after peptide injection.

In order to determine the adsorption kinetics of plasticins, $\gamma = f(t)$ relationships were used to calculate the first-order rate constants

k from the exponential adsorption equation, which relates the surface pressure to the adsorption time of a surfactant [22,26,27]:

$$e^{-kt} = \frac{\pi_{eq} - \pi_t}{\pi_{eq} - \pi_{t_0}} \quad (1)$$

where π_{eq}, π_t and π_{t0} are the surface pressures at equilibrium, at a given time t and at the initial time t_0, respectively.

2.2.2. Formation of lipid monolayers

Surface pressure-area π-A measurements of the lipid monolayers were performed using a thermostated Langmuir film trough (775.75 cm^2, Biolin Scientific, Finland) enclosed into a Plexiglas box. Solutions of phospholipids and LPS in chloroform-methanol 9:1 (v/v) were spread onto buffer. Prior to monolayer spreading, the subphase surface was cleaned by suction. After deposition, the system was left for 20 min to allow complete evaporation of the organic solvents. Compression was then performed at a speed of 5 $Å^2 \cdot molec^{-1} \cdot min^{-1}$. All experiments were run at 22 °C, and the results reported are mean values of at least three measurements. The surface compressional moduli K of monolayers were calculated, using Eq. (2):

$$K = -A\left(\frac{d\pi}{dA}\right)_T. \quad (2)$$

According to Davies and Rideal [24], K values below 12.5 mN/m, in the range 13–100 mN/m, 100 to 250 mN/m and above 250 mN/m would account for the gaseous state, the liquid expanded state (LE), the liquid condensed state (LC) and the solid state of a monolayer, respectively.

2.2.3. Assessment of peptide penetration into monolayers

Penetration of peptides into the lipid (LPS or PL) monolayer was inferred at constant area from the change in the surface pressure Δπ, recorded upon injection of a peptide solution beneath a lipid monolayer compressed to an initial surface pressure π_i between 5 and 40 mN/m. The maximal monolayer initial surface pressure π_i^{max} is deduced from the intersection of the data fitting lines and the horizontal x-axis, for which Δπ is zero. This pressure indicates the highest initial surface pressure above which the peptide is excluded from the interface [23,25]. Penetration of peptides into the lipid (LPS or PL) monolayer was also inferred at constant surface pressure from the change in the relative surface area ΔA/A versus time, recorded upon injection of a peptide solution beneath a lipid monolayer compressed to an initial surface pressure π_i of 40 mN/m. The pressure was maintained by a feedback loop that controls the barrier positions. The syringe containing the peptide solution was positioned beyond the barriers, allowing short injections at different locations beneath the preformed monolayer. The final peptide concentrations in the subphase were 0.1 or 1 μM. The results are mean values of at least three measurements.

2.2.4. Langmuir–Blodgett transfers

The Langmuir–Blodgett (LB) film transfer was performed on a Langmuir trough (KSV Biolin, Finland) equipped with a PTFE well. Firstly, freshly cleaved mica surfaces (1.5 × 1.5 mm^2) were attached on the dipper for LB film transfer of mixed LPS 3:1 monolayers. The clean substrate was immersed into buffer subphase, and then the LPS solution was spread onto the subphase. After solvent evaporation, the barrier was compressed at a constant rate (5 $Å^2 \cdot molec^{-1} \cdot min^{-1}$) and the π-A isotherm was simultaneously recorded. When the desired surface pressure (40 ± 1 mN/m) was reached and maintained constant by a feedback loop (±0.2 mN/m), the peptide was injected underneath the monolayer and relative area change was recorded. Once a steady state was obtained, the substrate was slowly lifted from the subphase (1.0 mm/min), allowing the LB transfer of the mixed LPS monolayer onto the mica substrate, while the surface pressure was still maintained at 40 mN/m. The LB-transferred mica surfaces were immediately glued onto a glass slide for further AFM imaging.

2.2.5. Brewster angle microscopy (BAM)

The morphology of monolayers spread at the air/buffer interface at $\pi_i = 40$ mN/m, before and following plasticin injection (final concentration: 0.1 μM or 1 μM) was monitored by Brewster angle microscopy (MicroBAM 3, Nima Technology Ltd., Coventry, UK). The microscope was equipped with a frequency laser diode (λ = 659 nm, 30 mW optical power) generating a collimated beam of approximately 6 mm diameter, with a p-polarizer, analyzer, and a USB camera. The spatial resolution of the BAM was about 6 μm per pixel, with a field of view of 3.6 × 4.1 mm^2, resolved over 640 × 480 pixels. Image size was 2.0 mm^2 after rescaling.

2.2.6. Liposomes preparation, DLS and zeta potential measurements

Liposome formulations made of either pure LPS Re 595, the mixture 3:1 (S-LPS/LPS Re 595), or the ternary PL mixture (SOPE/SOPG/CL 80:15:5) were prepared according to the Bangham's method followed by extrusion of vesicles suspensions [27–29]. Briefly, LPS was dispersed into a mixture of chloroform and methanol (9:1 v/v) at a concentration of 1.0 mg/ml. The ternary PL mixture (1.66 mM) was prepared in pure chloroform. Both organic solutions were evaporated for 3 h at 60 °C under reduced pressure, and the resulting dry lipid films were hydrated with buffer and sonicated for a few minutes. The obtained LPS or SOPE/SOPG/CL liposome suspensions were then extruded 10 times successively through 400 and 200 nm pore-diameter polycarbonate membranes at 50 °C (Mini extruder, Avanti Polar Lipids, Alabaster, AL). The diameter of liposomes (size in nm and polydispersity index PDI) was measured by diffusion light scattering (DLS) using a Zeta-sizer (Nano ZS90, Malvern) after dilution of the suspension in buffer. For zeta potential measurements, 0.05 ml of liposome suspension in buffer was diluted in 1 ml of a 477 mM glucose solution compensating for the reduction in ionic strength. All zeta potential and DLS measurements were carried out at 25 °C.

2.2.7. Assessment of the interaction between plasticins and liposomes

Prior to the experiments, the diameters of vesicles and plasticin aggregates were measured independently by DLS, and their specific turbidity with concentration was determined at 290 nm using a double-beam spectrophotometer (Lambda 35, Perkin-Elmer). A 20 μM peptide suspension (1.5 ml) was placed into a 1-cm optical quartz cell thermostated at 25 ± 0.5 °C and equipped with a rotation speed-controlled magnetic stirrer that did not interfere with the light path. LPS Re 595 liposomes in buffer (1 mg/ml, 170 μl) were added to the peptide suspension. The interaction between LPS Re 595 liposomes and plasticins was monitored by DLS, and by continuous absorbance measurement at 290 nm. The measurements were performed 2, 20 and 40 min following the beginning of liposome-peptide incubation.

2.2.8. Circular dichroism measurements

CD spectra were recorded with a Jobin Yvon CD6 dichrograph (Jobin Yvon, Palaiseau, France). The instrument outputs were calibrated with D(+)-10-camphorsulfonic acid. Spectral measurements were made over a range of 185–260 nm, with 5 $nm \cdot min^{-1}$ scan speed at 22 °C, and 1 nm-band width using a 2 mm path-length cell (Hellma France). Typically, five scans were accumulated and averaged. The CD spectrum of each peptide was recorded in 10 mM phosphate buffer (pH 7) and the peptide concentration was 25 μM. Then, the spectra were acquired in the presence of the three liposome models at a lipid concentration of 1.5 mM in 10 mM phosphate buffer to achieve a P/L ratio of 1/40. All dichroic spectra were corrected by subtraction of the background obtained for each peptide or lipid mixtures. CD measurements were reported as $\Delta\varepsilon$ ($M^{-1} \cdot cm^{-1}$) per residue. Deconvolution of CD spectra was achieved with Dichroweb [30] and CDNN [31] programs.

2.2.9. GIXD measurements under synchrotron radiation on LPS monolayers

X-ray scattering measurements were taken on the SIRIUS beamline at the SOLEIL Synchrotron. Its optics is described elsewhere [32]. The incident X-ray energy used was 10 keV ($\lambda = 1.24$ Å), and the beam size was 0.1×1 mm^2 at the sample position. The water surface was illuminated at an incident angle of 1.8 mrad below the critical angle of the air-water interface (2.15 mrad at 10 keV), so that the incident wave was totally reflected, while the refracted wave became evanescent, exploring a layer of several nanometers beneath the interface, and data were collected on a very low noise, position sensitive 1D gas detector, with 2048 channels on 150 mm. A custom-built Langmuir trough was enclosed in a temperature-controlled sealed chamber flushed with helium during data collection to reduce the gas scattering and to avoid beam damage to the monolayer. The aqueous subphase was cooled down to 10 °C during all experiments. After spreading, the lipid film was left for 30 min to allow for solvent evaporation and film relaxation, and then compressed at the speed of 5 Å$^2 \cdot$molec$^{-1} \cdot$min^{-1} until reaching ~40 mN/m [33]. The interaction with the peptides (0.1 and 1 μM) was studied at the constant surface pressure 40 mN/m.

Grazing incidence X-ray diffraction (GIXD) was used to obtain in-plane information about the molecular structure of the surface. Spectra were obtained by varying the X-ray momentum transfer in-plane component $Q_{||}$ that is parallel to the air–aqueous interface. The scattered intensity was measured as a function of the angle 2θ between the incident and diffracted beam projected onto the horizontal plane. GIXD data were reduced by the background, polarization and Lorentz corrections, as well as the change in illuminated area by the X-ray beam. Diffraction peaks (integrated intensity against $Q_{||}$) were fitted with Lorentzian curves and the peak position values were used to obtain unit-cell dimensions of the lipid lattices. Their angular position $2\theta_{hk}$, corresponding to $Q_{hk} = (4\pi/\lambda) \sin 2\theta_{hk}/2$, yielded the distance $d_{hk} = 2\pi/Q_{hk}$ for the two-dimensional (2D) lattice structure. They could be indexed by the two Miller indices h and k yielding the 2D unit cell. Full-width at half maximum (FWHM) values determined from the adjustment were used to determine the in-plane correlation length from the Scherrer formula in the case of Lorentzian shape peaks [34]: $L = 2/\text{FWHM}\ (Q_{||})$, where FWHM ($Q_{||}$) is the resolution corrected full-width at half-maximum in $Q_{||}$ units. The correlation length gives the spatial extension of the crystalline domains existing in the monolayer. Intensity distribution along the out-of-plane component Q_z for the main Bragg peaks (rod scans) fitted with a sinus cardinal functions provided an estimate of the diffracting layer thickness L_z through the equation $L_z = 2/\text{FWHM}\ (Q_z)$, as well as the tilt and azimuthal angles t and ϕ of lipid molecules with respect to the normal to the air/buffer interface and to the in-plane axis of the unit cell: $(\tan(t).\cos(\phi) = Q_z^{max}/Q_{||}^{max})$.

2.2.10. Atomic force microscopy experiments

AFM experiments were performed with a JPK Nanowizard 3 Ultra Speed from JPK Instruments (Berlin, Germany, www.jpk.com). The microscope was located on an air-buffered table coupled to a dynamic anti-vibration device and enclosed in an acoustic box. Because of its plate like structure composed of an octahedral alumina sheet sandwiched by two tetrahedral silicate sheets, the cleavage of muscovite mica surface reveals a molecular smooth surface. Mica substrates with surface area of 1.5×1.5 cm^2 were used. Imaging of LB-transferred monolayers on mica was performed in air in AC-HyperDrive® mode (phase modulation), with gold coated silicon cantilevers PPP-NCHAuD of 40 N/m spring constant and 290 kHz resonance frequency (Nanosensors, Neuchatel, Switzerland). The pyramid-shaped tips had a radius of curvature less than 10 nm. A free amplitude oscillation of 1 nm was chosen allowing a very high resolution of the imaged surface. Images were taken at the scan rate of 1 Hz. Image processing (flatten, plane fit, edge and line detection) was performed with the JPK Data Processing software (JPK Instruments). At least three different areas of each sample were scanned and typical images were presented. Average values of height and lateral dimensions of domains were determined with all domains detected in the picture.

3. Results and discussion

The two plasticins were first studied in solution to analyze their interfacial behavior, and then in contact with various lipid models of the bacterial OM, in order to examine their state of aggregation, conformation and ability to penetrate and disorganize condensed LPS monolayers.

3.1. Behavior of plasticins at the air/buffer interface

Fig. 1 shows the surface pressure at equilibrium–concentration relationships for each plasticin injected into buffer.

Both plasticins adsorbed at the air/solution interface, although the cationic PTCDA1-KF lowered more the surface tension than PTCDA1, and diffused 5-fold faster towards the interface at 0.1 μM and 5.8-fold at 1 μM (Table 1). The critical aggregation concentration (cac) was estimated to 0.14 ± 0.01 μM for both plasticins. Beyond this similarity, the replacement of three amino acids in the PTCDA1 primary sequence, among which two of them are positively charged, induced a difference in the interfacial behavior between the two plasticins. At 0.1 μM, the surface activity of the natural plasticin was negligible: 0.5 ± 0.7 mN/m, whereas that of the modified plasticin reached 10.2 ± 3.1 mN/m. Earlier observations by Brewster angle microscopy (BAM) showed that plasticins below their cac formed small domains (50–100 μm in size) with irregular shapes after 2 h adsorption at the free air/buffer interface [12]. Above the cac, at 1 μM, both plasticins are highly surface active, with a surface pressure at equilibrium of 31.9 ± 0.5 mN/m for the natural plasticin and up to 38.9 ± 0.5 mN/m for the cationic one.

Polymyxin B (PMB) was chosen for comparison and appeared to be much less tensioactive than the plasticins, and diffused to the interface 10-fold slower than PTCDA1.

DLS measurements performed on 1 μM PTCDA1 suspensions revealed a broad spectrum centered on very large diameters (>5 μm). Sedimentation was observed in the cuvette. At the same concentration for PTCDA1-KF the intensity spectrum appeared very polydisperse with the coexistence of very small objects (a few tens of nm), larger ones (a few hundreds of nm) and very large aggregates (>4 μm). However, when expressed in volume, the main fraction (>70%) corresponded to the very small objects. The modified plasticin thus seemed to aggregate to a lesser extent than the native one and formed oligomers of smaller sizes, which could explain the higher surface pressure at equilibrium of its solutions and higher adsorption rates.

Circular dichroism showed that both peptides were mainly unordered in solution, with a strong β-sheet component (~45%), as inferred from the presence of a negative band located at 207 nm (Fig. 2 and Supplementary information S1). This conformation is in agreement with literature data [35], and could explain the strong tendency of both peptides to aggregate in aqueous solution observed by DLS.

3.2. Assessment of plasticins interaction with liposomes by circular dichroism, DLS and turbidity measurements

DLS and turbidity experiments were performed to monitor changes in the aggregation pattern of plasticins upon their interaction with liposomes. DLS measurements of PL, LPS Re 595 and LPS 3:1 liposome suspensions before incubation with the peptides showed homogeneous populations of unilamellar[1] vesicles with similar sizes: ~190 nm (PDI 0.10), ~175 nm (PDI 0.13), and ~150 nm (PDI 0.18) for PL, LPS Re 595 and LPS 3:1 vesicles respectively. The corresponding zeta potential (ζ) values were −46.4 ± 1.5, −50.4 ± 3.9 and −12 ± 1.9 mV. They

[1] Cryo-transmission electron microscopy experiments confirmed that both extruded PL and pure LPS Re 595 liposomes were effectively unilamellar (data not shown).

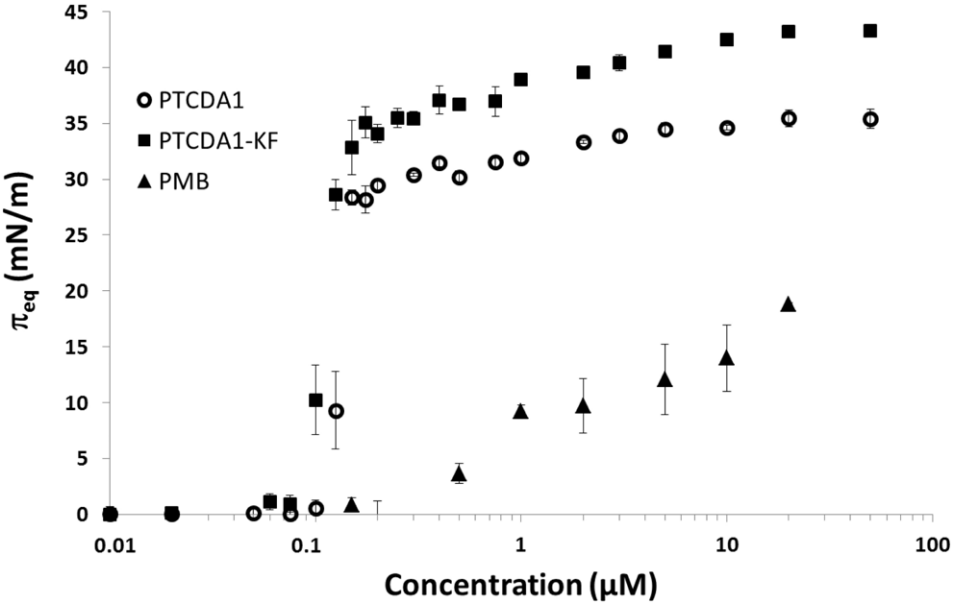

Fig. 1. Surface pressure at equilibrium π_{eq} vs. concentration for the native peptide PTCDA1 (open circles), the cationic PTCDA1-KF (filled squares) and polymyxin B (PMB, filled triangles) injected into buffer.

were all negative, as expected from the presence of negatively charged LPS, SOPG and CL. However, the presence of the smooth strain (S-LPS) led to less negative vesicles, probably due to charge screening by the long oligosaccharide chains.

When 1 μM PTCDA1 aggregates were put in contact with LPS Re 595 liposomes, DLS measurement showed the coexistence of vesicles (~180 nm, PDI 0.20) and peptide (or peptide-liposome) aggregates of several microns in size. The absorbance measured at 290 nm increased, but the final value (0.22) corresponded to the sum of absorbance of the peptide (0.09) and liposomes measured separately (0.11). This result indicates that the native peptide PTCDA1 did not disaggregate upon interaction with the LPS liposomes. Conversely, addition of PTCDA1-KF to LPS Re 595 liposomes led to the total disappearance of the polydisperse spectrum of the cationic plasticin. A fine unique peak was observed, corresponding to a homogeneous population of vesicles with slightly larger sizes than before peptide addition (~200 nm, PDI 0.15). Turbidity measurements confirmed these observations, showing a sharp fall in the absorbance (0.25 for the peptide before interaction, 0.12 after interaction with LPS liposomes), which then corresponded to that of LPS liposomes alone (0.11): the cationic plasticin disaggregated into small oligomers upon interaction with the vesicles, and inserted into their bilayers, however without destabilizing them. The same trend was observed with PL liposomes.

CD measurements (Fig. 2) showed that in the presence of both pure mutant LPS Re 595 and mixed LPS 3:1 liposomes, PTCDA1 remained fully unordered, whereas PTCDA1-KF became highly α-helix structured (~60%), as demonstrated by the presence of a negative double band centered at 209 and 222 nm (Fig. 2B). In contact with PL vesicles, unordered state of PTCDA1 coexisted with minor β and α structures (Fig. 2A), while PTCDA1-KF remained mainly unordered, with a lower α-helix component.

The natural plasticin PTCDA1 and its modified counterpart PTCDA1-KF differ by their charge and conformation. PTCDA1 is almost neutral with a slightly negative charge (−0.02) and is mainly disordered in buffer at micromolar concentrations [11], whereas PTCDA1-KF is cationic (+2) and mainly structured as amphipathic α-helices oligomers. It is obvious that for the neutral PTCDA1, electrostatic interactions between molecules were very weak and hydrophobic interactions dominated. This probably explains the formation of the large aggregates in suspension and/or their sedimentation in the aqueous phase. On the contrary, for PTCDA1-KF, the electrostatic repulsion between cationic residues of α-helices was probably competing with the attractive van der Waals interactions between non-polar ones, which made the aggregation pattern more polydisperse with small oligomers (a few hundreds of nanometers) coexisting with larger sedimenting aggregates. The combination of CD, DLS and turbidity measurements clearly demonstrated the ability of the cationic peptide to disaggregate and adopt a α-helix structure upon interaction with the LPS above 1 μM concentration. This plasticin interacted as small oligomers of α-helices with the LPS bilayer. The inactive plasticin remained predominantly unordered and aggregated in contact with all bacterial lipids. Clearly, the two plasticins behaved differently and were not in the same physical state during the initial steps of the interaction with the OM.

In order to study the effect of the peptides on the organization of the lipids, we formed monolayers at the air/buffer interface and injected PTCDA1 and PTCDA1-KF beneath them. The changes in organization were analyzed by surface pressure-area measurements, GIXD and AFM experiments.

Table 1
Surface pressure at equilibrium and first-order rate constants of peptide adsorption, as calculated using Eq. (1).

Free interface	PTCDA1		PTCDA1-KF		PMB	
	0.1 μM	1 μM	0.1 μM	1 μM	0.1 μM	1 μM
Surface pressure π_{eq} (mN/m)	0.5 ± 0.7	31.9 ± 0.5	10.2 ± 3.1	38.9 ± 0.5	1.9 ± 0.5	9.7 ± 0.6
First order rate k_1 (min^{-1})	2×10^{-3}	1.1×10^{-1}	1.0×10^{-2}	7.4×10^{-1}	10^{-4}	1.1×10^{-2}
First order rate k_2 (min^{-1})	–	2×10^{-2}	–	6×10^{-3}	4.1×10^{-3}	–

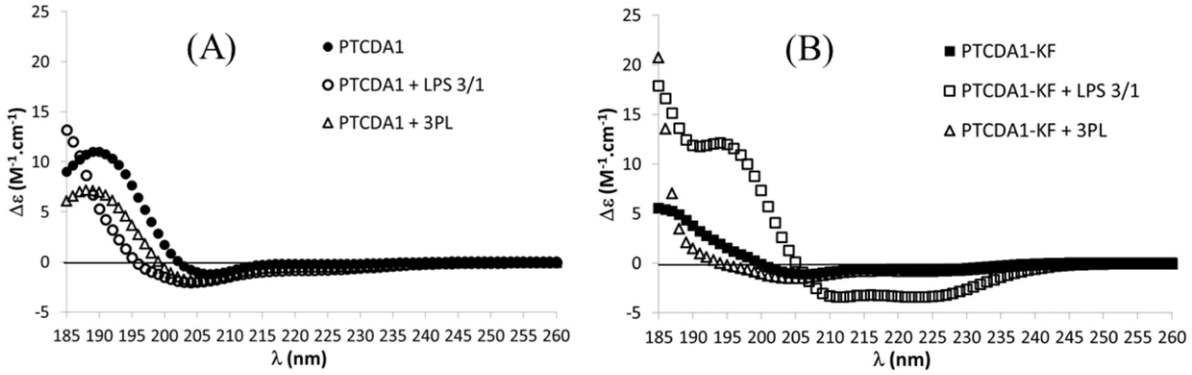

(C)

Peptide	Alone in PBS	+LPS Re 595	+LPS 3:1	+3PL
PTCDA1	**U** + β	**U**	**U**	**U** +α + β
PTCDA1-KF	**U** + β	**α**	**α**	**U** + α

Fig. 2. Circular dichroism spectra obtained for each peptide: the native plasticin PTCDA1 (A) and the cationic plasticin PTCDA1-KF (B) alone in 10 mM phosphate buffer (pH 7) and in interaction with LPS 3:1 and ternary PL liposomes. (C) Deconvolution of CD spectra revealing the different components of the secondary structures of peptides: "U" for unordered, "α" for α-helix structures and "β" for β structures (sheets and turns). Major components (>50%) are displayed in bold.

3.3. Assessment of peptide effect on the organization and structure of LPS and PL monolayers

3.3.1. Model LPS monolayers

In agreement with recently reported data for *Escherichia coli* smooth strain LPS [20], we were not able to form stable monolayers of smooth strain LPS (S-LPS) from *S. enterica*. The long hydrophilic oligosaccharide chains lead to S-LPS solubilization into the subphase. To check this hypothesis, the deposited mass of smooth strain LPS was varied from 100 μg to 1000 μg, and we calculated the work of compression W_C (inset to Fig. 3). It increased linearly from 0 up to 0.4 J for 500 μg LPS. The plot failed to cross the zero coordinate because of a fraction of the initially deposited LPS molecules was lost into the subphase [21]. The linear increase of the W_C–smooth strain LPS amount relationship indicated that above 111 μg, LPS molecules could organize in a monolayer and sustain dynamic compression. However, the highest surface pressure reached was 20 mN/m corresponding to a very low mass area (below 0.1 m^2/mg), suggesting solubilization of molecules into the buffer subphase during compression.

Contrarily to S-LPS, which formed unstable and disorganized monolayers (K_{max} <50 mN/m), the mutant LPS Re 595 remained stable in monolayer at the air/buffer interface (Fig. 3) [36,37]. It collapsed at

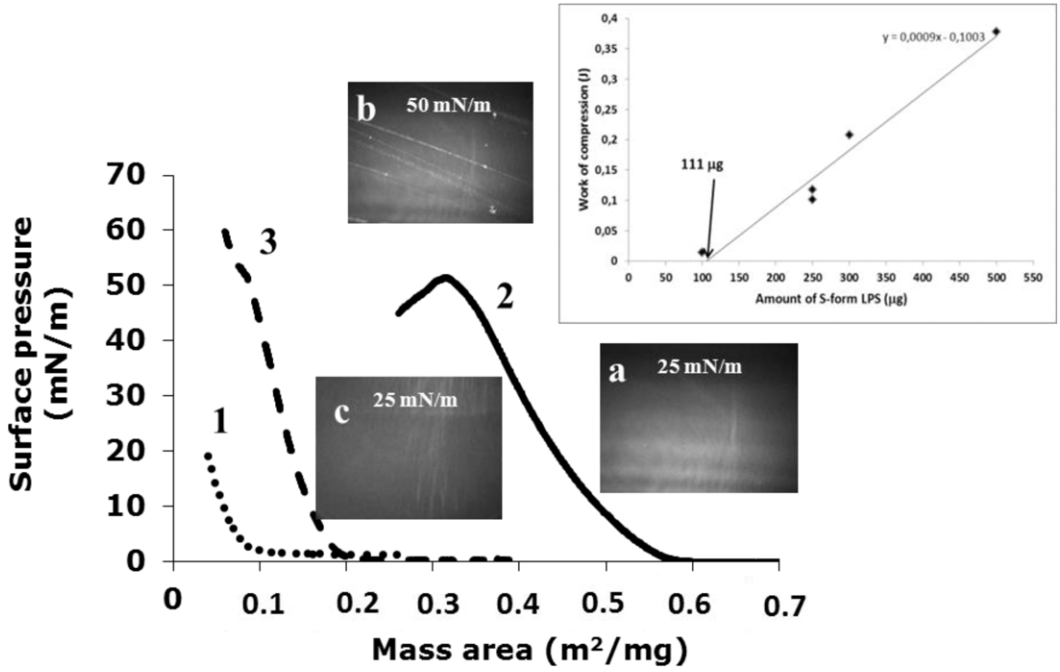

Fig. 3. π-A isotherms and associated BAM images of smooth strain LPS monolayer (300 μg, dotted curve 1), pure rough mutant strain LPS Re 595 monolayer (160 μg, plain curve 2, images a and b), and (3:1) mixture of smooth strain LPS and rough strain LPS Re 595 monolayer (200 μg, dashed curve 3, image c). Inset: plot of the compression work of smooth strain LPS monolayers on buffer versus the amount of molecules deposited.

51.5 mN/m and surface compressional modulus-surface pressure relationships indicated that this monolayer was in a liquid-condensed state in the 20–44 mN/m surface pressure range (K_{max} was 131.5 mN/m at 30 mN/m). BAM observation revealed the presence of bright spots at 35 mN/m, accounting for the beginning of a 3D organization of the monolayer through a nucleation mechanism [38]. Above 40 mN/m, white stripes resulting from the merging of nuclei of condensation appeared (see image "b" in Fig. 3).

A mixture of smooth strain LPS and rough mutant strain LPS Re 595 molecules (3:1 mass ratio) allowed the formation of stable monolayers. Deposition of 200 μg was sufficient to obtain full reproducible isotherms (Fig. 3). The pure rough strain LPS and the 3:1 mixture collapsed at 51.5 mN/m and 59.2 mN/m, respectively. Such an increase in surface pressure at collapse is an indication of molecular interactions between the two LPS.

The mixed LPS 3:1 monolayer appeared completely homogeneous upon compression under the Brewster angle microscope (image "c" in Fig. 3): no macroscopic nucleus of condensation neither stripe was observed, except at collapse. These results suggest that the two LPS species were miscible. The mixed LPS monolayer was less organized (K_{max} = 97.3 mN/m) than the pure mutant LPS Re 595 one, but much more than the pure natural S-LPS one.

In order to check the stability of the mixed LPS 3:1 monolayer, we performed compression–expansion cycles until the surface pressure of 40 mN/m (Fig. 4). They showed only 11% loss in area following the second cycle. Further cycle overlapped with the first one demonstrating the good stability of this monolayer.

Moreover, all cycle isotherms intersected at the same area at the surface pressure of 40 mN/m even if they did not go back to full zero pressure after the first compression (~+ 1.8 mN/m). This result indicates that a dynamic equilibrium between the interface and the bulk maintained the same mass of LPS molecules at the interface at high surface pressure.

The mixed LPS 3:1 monolayer was considered as a relevant external leaflet model since it contained LPS in its natural form with full mobile and flexible oligosaccharide chains immersed in the aqueous subphase. It appeared thus as a relevant biomimetic model of the outer leaflet of the bacterial OM to study plasticins penetration.

3.3.2. Insertion experiments at constant surface area

Fig. 5 shows the surface pressure increments (Δπ) with respect to the initial surface pressure of the mixed 3:1 LPS monolayer (π_i), upon injection of the two plasticins at 0.1 or 1 μM concentration.

Analysis of the adsorption–penetration curves showed evidence of a dissimilar behavior for the two plasticins in contact with the mixed LPS 3:1 monolayer. For each concentration studied, the absolute values of the curve slopes were generally higher for the cationic peptide than for the natural one. The $\Delta\pi$–π_i plot demonstrated the effective penetration of this plasticin into the monolayer at initial surface pressures similar to that observed in natural membranes, even at low concentrations (below the cac). The difference in slope between plasticins was less pronounced at 1 μM, due to the influence of their high surface activity on their adsorption/penetration process at concentrations higher than their cac. However, at the initial pressure of 40 mN/m, the natural plasticin was unable to induce increments of surface pressure, whereas the modified one could still produce a Δπ of 3.7 mN/m. The critical pressure of insertion (also called exclusion pressures) π_i^{max} for both plasticins also reflected the higher affinity of the cationic plasticin for the mixed LPS monolayer, especially at 1 μM concentration: they were within the range of lateral surface pressures observed in natural membranes for the natural plasticin at 1 μM (35.3 ± 3.0 mN/m), but clearly higher (42.5 ± 3.2 and 45.6 ± 3.9 mN/m at 0.1 and 1 μM respectively) for its cationic counterpart.

BAM examination of PTCDA1-KF insertion into the mixed 3:1 LPS monolayer revealed changes in monolayer morphology (Fig. 5). Large straight bands of white spots were observed a few minutes after injection of PTCDA1-KF at 1 μM, which merged together to form lines of nuclei of condensation. These morphology changes were probably due to peptide insertion into the mixed LPS monolayer and significantly contrasted with the homogeneous morphology of the mixed monolayer in the absence of peptide or in the presence of PTCDA1 at any concentration: PTCDA1 aggregates did not affect significantly the mixed LPS to generate any contrast at the interface. This observation suggests that they remained adsorbed beneath the LPS monolayer.

Thus, the surface pressure of 40 mN/m appears to be a pivot value in the penetration pattern of the two plasticins and was chosen as the initial surface pressure at which further insertion experiments have been performed.

3.3.3. Insertion experiments at constant surface pressure

As a natural membrane can also expand to accommodate the penetration of a peptide, insertion experiments in the constant pressure mode have been performed with two model monolayers compressed to the initial surface pressure of 40 mN/m: the mixed LPS 3:1 monolayer and a pure SOPE neutral monolayer to examine the contribution of hydrophobic and electrostatic interactions between the plasticins and the lipid molecules. Fig. 6 presents the relative area increase with respect to time after injection of plasticins into the subphase beneath these monolayers.

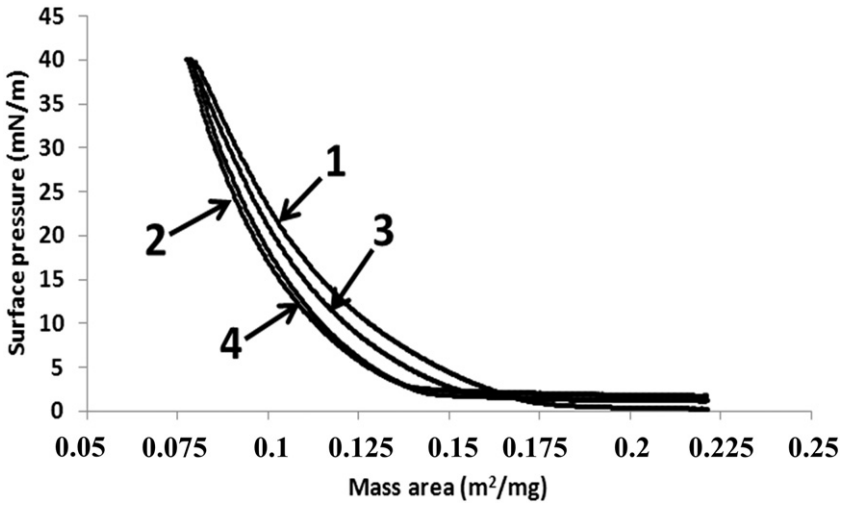

Fig. 4. Compression–expansion of the LPS 3:1 monolayer until the surface pressure of 40 mN/m on buffer subphase. 1: first compression, 2: first expansion, 3: second compression and 4: second expansion, all performed with 350 μg of LPS 3:1 mixture spread and compressed at the speed of 5 $Å^2 \cdot molec^{-1} \cdot min^{-1}$.

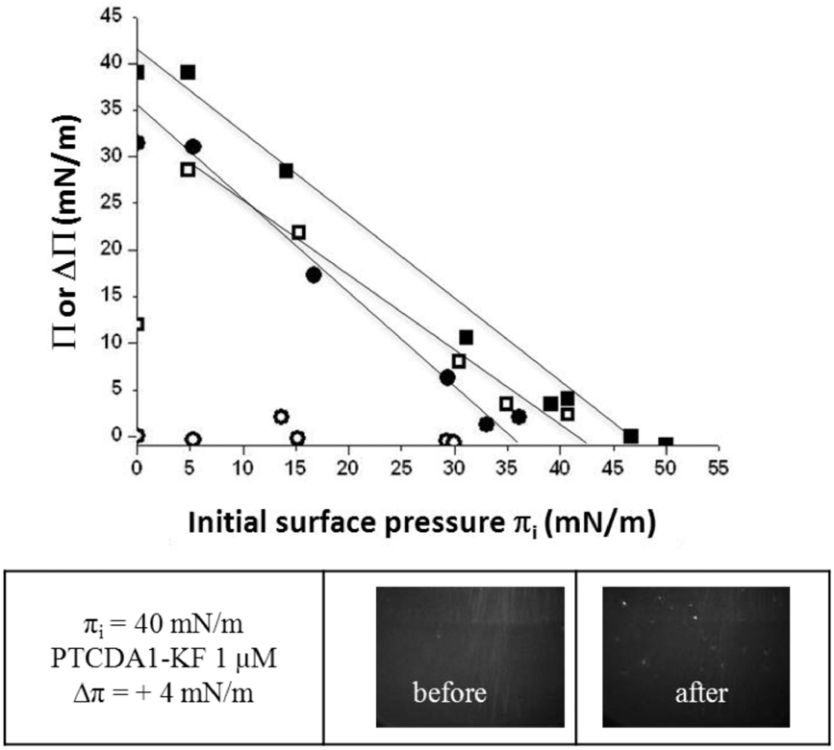

Fig. 5. (Above) $\Delta\pi$–π_i relationships in the constant area mode induced by the injection of PTCDA1 at 0.1 µM (○) and 1 µM (●) and PTCDA1-KF at 0.1 µM (□) and 1 µM (■) beneath the mixed LPS 3:1 monolayer. (Below) BAM images of the mixed LPS 3:1 monolayer initially compressed at 40 mN/m before, and following injection of the modified plasticin at 1 µM into the subphase.

At 0.1 µM concentration, the natural plasticin PTCDA1 (Fig. 6A) was unable to penetrate the anionic mixed LPS monolayer, and barely interacted with the neutral SOPE monolayer ($\Delta A/A$ ~+5.46 ± 1.2%). At 1 µM concentration, the kinetics were as long as 50 min after PTCDA1 injection to reach equilibrium, but the aggregates of the natural plasticin could induce significant area increase in the SOPE monolayer (+36.7 ± 3.6%). Knowing that PTDA1 at 1 µM can induce a surface pressure of 32 mN/m at the free interface, such an area increase in a monolayer constantly maintained at the surface pressure of 40 mN/m demonstrates the contribution of hydrophobic interactions with the SOPE molecules in the adsorption/penetration process.

The kinetics of area increase was different for the mixed LPS 3:1 monolayer. A transient higher adsorption regime (~+13%) was observed 25 min after injection, before a decrease to the final value of +3.7 ± 0.9% obtained 40 min after injection. This behavior may be due to a reorganization of the peptide aggregates beneath the monolayer that finally altered their ability to penetrate into the condensed LPS monolayer. It is also possible that the repulsive electrostatic interactions between the strongly anionic LPS headgroups and the slight negative charge of the peptide (−0.02) overcame the hydrophobic interactions and hindered the penetration of PTCDA1 into the negatively charged monolayer.

A strikingly different insertion behavior was observed for the cationic plasticin (Fig. 6B). At 0.1 µM concentration, the cationic plasticin PTCDA1-KF was able to induce an area increase of 35 ± 2.0% with the anionic mixed LPS monolayer whereas only 13 ± 4.3% was measured with the neutral SOPE one. This difference demonstrates the role of the attractive electrostatic interactions between the polar LPS headgroups and the lysine residues of the cationic plasticin. Above the cac, at 1 µM, the relative area increase was 62 ± 5.1% with SOPE monolayer, but reached 69 ± 2.6% with the mixed LPS one after 20 min following injection. After 20 min the compression barriers reached their stop position after a full expansion, which explains the sudden plateau observed. Extrapolation of this curve gave a relative area increase of 80% after 40 min following the injection. If one takes into account the high surface activity of the cationic plasticin that can induce surface pressure equivalent to the one existing in the monolayer, such an area expansion of the monolayer at 40 mN/m resulted not only from the electrostatic adsorption of the peptide to the polar head groups of the anionic LPS monolayer, but also from its effective insertion between the LPS molecules at the interface.

Thus, peptide insertion experiments allowed discrimination of the two plasticins. They demonstrated that their adsorption/penetration beneath the mixed LPS monolayer was driven by both electrostatic and hydrophobic interactions. In the presence of the mixed LPS 3:1 monolayer, the cationic plasticin induced more significant changes than the natural one, demonstrating the influence of the peptide charge.

To get a better insight into the effect of plasticins on the structure of LPS monolayers, GIXD measurements using synchrotron radiation and AFM imaging were performed on mixed LPS 3:1 monolayers at constant surface pressure.

3.3.4. GIXD measurements

Monolayers of pure mutant LPS Re 595 from *S. enterica* can generate a GIXD signal only at low temperature (Supplementary information S3) [39]. Figs. 7A and 8A present typical GIXD data obtained for the mixed 3:1 S-LPS/LPS Re 595 monolayer on buffer subphase at 10 °C, and compressed to 40 mN/m. As shown in Table 2, data analysis yielded two Bragg peaks in the condensed phase at $Q_{||}$ positions 1.46 and 1.51 $Å^{-1}$, with corresponding d-spacings 4.3 and 4.2 Å respectively. Knowing that the LPS species from *S. enterica* contain in average up to seven hydrocarbon chains, we choose to discuss the results by using an oblique hexagonal unit cell of which dimensions were a = 4.8 Å, b = 5.0 Å and $\gamma = 113°$. The peaks were then indexed as (10) and (01) respectively. The primitive cell area for the mixture was slightly larger (21.6 $Å^2$) than for the pure mutant LPS monolayer (20.7 Å, see Supplementary information S3), probably due to the presence of the large polar headgroup of the smooth LPS. The area per LPS molecule was 140.2 $Å^2$. This value is close to the one deduced from the surface pressure-area isotherms at 40 mN/m (141.5 $Å^2$).

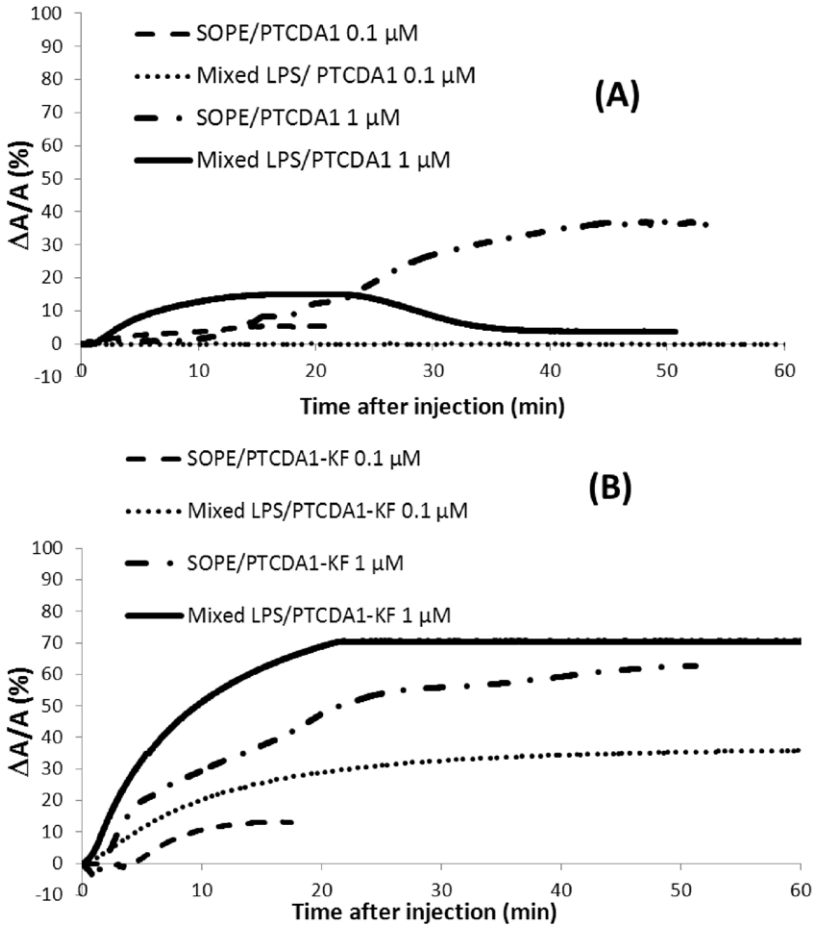

Fig. 6. Relative surface area change (%) upon injection of PTCDA1 (A) and PTCDA1-KF (B) at 0.1 and 1 μM concentrations beneath the mixed LPS 3:1 monolayer (dotted and plain curves), and the pure SOPE one (dashed and dashed-dotted curves).

The in-plane correlation lengths corresponding to the (10) and (01) Bragg peaks were 30 and 568 Å respectively, values that have to be compared with those measured for the pure mutant LPS monolayer (37 and 300 Å respectively, Supplementary information S4). The presence of the smooth LPS in the monolayer increased the order extension of the (01) Bragg peak. Smooth and mutant LPS differ only by their polar part, and GIXD signal is mainly sensitive to the crystalline organization of all hydrocarbon chains that are identical between the two molecular species present in the 3:1 LPS mixture.

Fig. 8B shows the 2D contour plots (intensity versus $Q_{||}$ and Q_z) of the mixed LPS monolayer alone. Analysis of the (10) rod profile provided: (i) a crystalline thickness for the mixed LPS monolayer of 14 Å which corresponds, as expected, to stretched C14 hydrocarbon chains, and (ii) no tilt angle for the two LPS species with respect to the normal of the interface since the out-of-plane component of the two Bragg peaks was negligible.

Interaction with the plasticins yielded GIXD spectra that demonstrated a clear discrimination in their effect on the mixed LPS monolayer organization. As expected, the GIXD spectrum obtained after interaction with the natural plasticin PTCDA1 at the 0.1 μM concentration displayed the two Bragg peak at $Q_{||}$ positions 1.36 $Å^{-1}$ and 1.51 $Å^{-1}$ (Fig. 7B), with corresponding d-spacings 4.6 and 4.2 Å, 20% reduced intensity and lower in-plane correlation length for the (01) Bragg peak, demonstrating a slight modification of the mixed LPS monolayer structure and a decrease of the amount of organized matter below the X-ray footprint.

Above the cac, at 1 μM concentration, Fig. 8C shows that the natural plasticin induced more damage to the LPS monolayer structure since: (i) the fine (01) Bragg peak vanished, and (ii) the unit cell dimensions became identical at 5.1 Å (Table 2). These results demonstrate a partial disorganization of the mixed LPS monolayer, mainly due to the plasticin adsorption beneath the monolayer.

Our previous surface pressure-area measurements performed in the constant pressure mode confirmed the effective insertion of the cationic plasticin at both concentrations into the mixed LPS monolayer at an initial pressure of 40 mN/m. Here, at 10 °C, both S-LPS and LPS Re 595 are in their gel phase (T_m around 26 °C, DSC data not shown) and this physical state could delay the modifications in structure upon penetration of the cationic plasticin (or polymyxin B). However, this insertion pattern yielded to featureless GIXD spectra at both concentrations (Fig. 7D for the 0.1 μM concentration and Fig. 8D for the 1 μM one): the disappearance of the diffraction peaks demonstrated the complete disorganization of the hydrocarbon chains in the monolayer. In addition to the electrostatic adsorption of alpha helices to the LPS anionic polar groups that can affect the organization of the hydrocarbon chains, the effective penetration of the cationic plasticin into the monolayer at the level of the LPS aliphatic chains also contributed to the complete loss of structure of the biomimetic monolayer through a dilution effect.

For comparison, we tested the active cationic PMB against the mixed LPS monolayer. At 0.1 μM, PMB induced almost no change to the monolayer structure (Fig. 7 C), a behavior similar to that produced by the natural plasticin at this concentration. This result was expected since its minimal concentration required for inhibiting Gram-negative bacteria is slightly higher (0.25 μM). Conversely, at 1 μM, a concentration at which this polypeptide was weakly surface active (10 mN/m), the corresponding GIXD spectra appeared almost flat (data not shown) demonstrating that the active PMB, as the cationic plasticin, could deeply disorganize the mixed LPS monolayer structure.

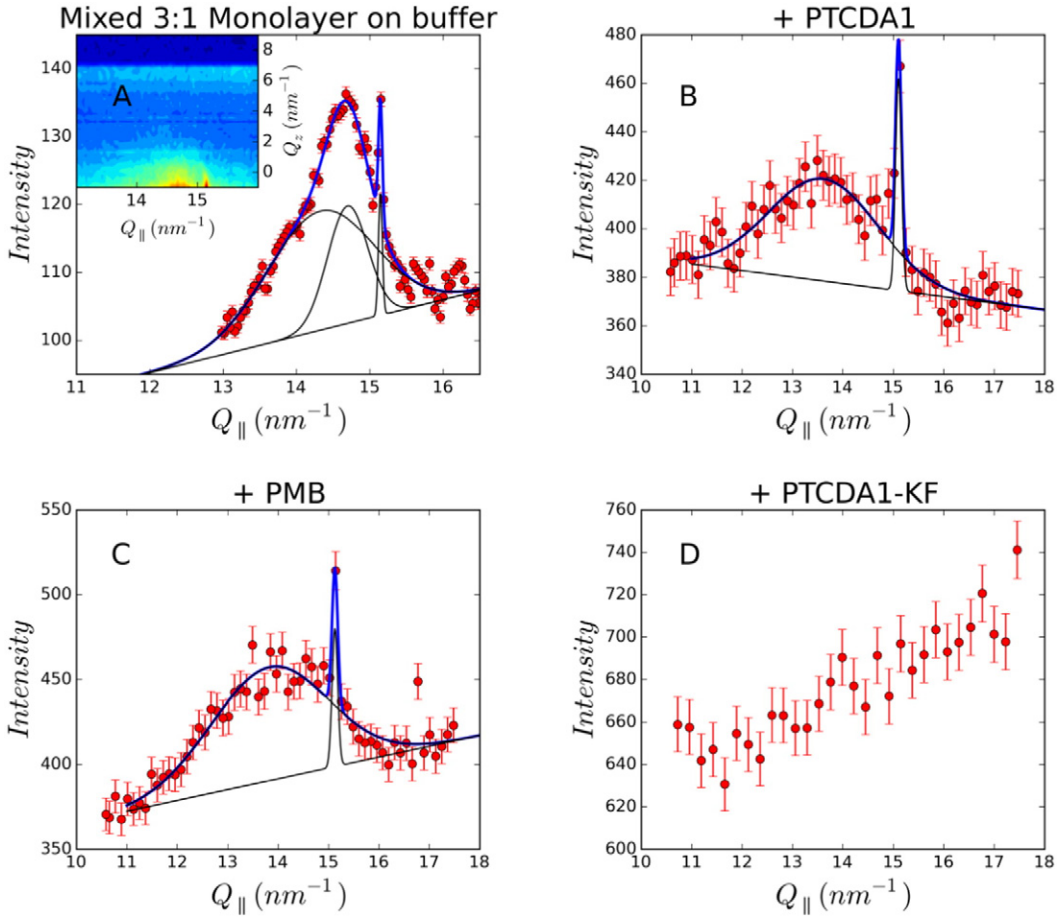

Fig. 7. GIXD spectra (intensity versus $Q_{||}$) obtained at 10 °C on buffer subphase of a mixed 3:1 S-LPS/LPS Re 595 monolayer compressed at 40 mN/m: (A) before interaction (the inset presents the 2D contour plots with intensity versus $Q_{||}$ and Q_z), (B) after interaction with PTCDA1 at 0.1 μM in buffer, (C) after interaction with PMB at 0.1 μM in buffer, (D) after interaction with PTCDA1-KF at 0.1 μM in buffer.

Gidalevitz et al. [16,17] studied the effect of the antimicrobial cationic peptide protegrin 1 on the in and out-of-plane structures of DPPC, DPPG and lipid A monolayers by X-ray diffraction measurements. They showed that protegrin 1 was able to disorganize mainly the anionic lipid films (PG and lipid A) through insertion into the monolayer and modification of the hydrocarbon chains packing.

GIXD experiments coupled to surface pressure measurements performed at constant pressure allowed thus discrimination of the two plasticins with mixed LPS monolayers. The native neutral peptide was ineffective at 0.1 μM, and barely interacted at 1 μM with the mixed LPS monolayer, whereas the cationic peptide inserted into it, even at surface pressures well above the surface pressures in natural membranes. Ultimately, the loss of organization in the hydrocarbon chains of the mixed peptide/LPS monolayer demonstrated the effective penetration of the cationic plasticin in the apolar part of mixed LPS monolayers. This would account for a synergic contribution of hydrophobic and attractive electrostatic interactions between cationic plasticin α-helices-structured oligomers and the LPS species, as already described for other short, cationic α-helical antimicrobial peptides such as cecropins and magainins [40] or cyclic ones such as polymyxin B [15].

Further AFM experiments were then performed to reveal the lipid organization in monolayers at the nanoscale level before and after interaction with plasticins, as well as the morphology of peptides aggregates.

3.3.5. AFM experiments

After compression of a mixed LPS 3:1 monolayer to 40 mN/m, a plasticin was injected into the subphase and the interaction was monitored at constant surface pressure until equilibrium in surface area was reached. The resulting system was then LB-transferred onto a freshly cleaved mica surface. AFM observations were performed in air in the AC-HyperDrive mode, the AFM tip thus imaging the apolar face of the monolayer. It was not possible to avoid the adsorption of some salt crystals from the buffer onto the surface.

3.3.5.1. AFM imaging of LB-transferred LPS monolayers before interaction. Fig. 9A shows an AFM picture of the LB-transferred mixed LPS monolayer before interaction with plasticins. Although this monolayer appeared fully homogeneous on BAM pictures, AFM pictures revealed its organization in domains at the nanoscale level. Small dark circular domains with irregular shapes coexist with a surrounding homogeneous lighter matrix. The difference in height between the two domains strongly depends on the force applied, but with forces ranging from 500 pN up to 1 nN, reproducible measurements could be obtained, and in average, the darker domains are 0.75 ± 0.1 nm lower than the surrounding phase. The spatial extension of the darker domains is in average 17.0 ± 2.1 nm, a value lower than that of domains found in pure mutant LPS Re 595 monolayer at similar surface pressures [37]. The corresponding phase image (data not shown) of the mixed monolayer showed a lower phase shift in the darker domains than the surrounding matrix, indicating a more fluid phase in the circular domains than in the higher phase. Based on these results [37], we can associate the darker domains to the liquid expanded (LE) phase of the LPS mixture and the surrounding higher phase to the liquid condensed (LC) phase of the monolayer.

3.3.5.2. AFM imaging of LB-transferred LPS monolayers after interaction with plasticins. Fig. 9B shows a typical AFM picture of the LB-

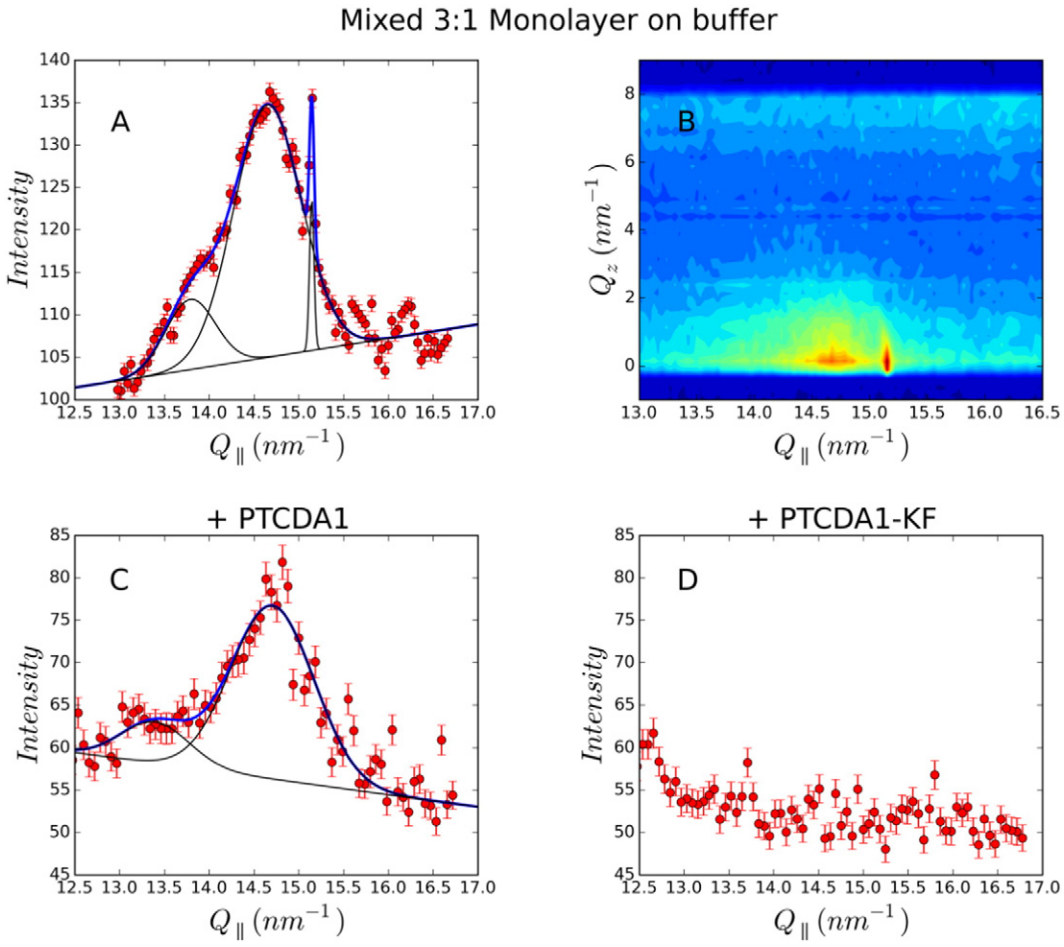

Fig. 8. GIXD spectra (intensity versus $Q_{||}$) obtained at 10 °C on buffer subphase of a mixed 3:1 S-LPS/LPS Re 595 monolayer compressed at 40 mN/m: (A) before interaction, (C) after interaction with PTCDA1 at 1 μM in buffer, (D) after interaction with PTCDA1-KF at 1 μM in buffer. (B) 2D contour plots (intensity versus $Q_{||}$ and Q_z) of the mixed LPS monolayer alone.

transferred mixed LPS monolayer after interaction with the natural plasticin PTCDA1 at 1 μM. The organization of the monolayer in LE and LC domains was fully preserved, but the number of LE domains decreased roughly by a factor 2 and their geometry was changed. Indeed, the difference in height between the two domains increased to 1.04 ± 0.14 nm (+38% as before interaction) and the spatial extension of the LE domains was in average 29.4 ± 3.7 nm, which represents an area increase of 73% with respect to the monolayer before interaction. Overall, the total area occupied by the LE phase remained globally the same as before interaction, but a reorganization of the LE phase occurred upon interaction with the natural plasticin. This result has to be related to the small relative area increase (+3.7%) observed in surface pressure measurements. Clearly, PTCDA1 at 1 μM modified the nanoscale organization of the LPS monolayer, particularly the LE phase.

Interaction with PTCDA1-KF at 1 μM yielded the AFM pictures presented in Fig. 10A and B. The ratio transfer of this monolayer was less than 10%. Very few patches of the monolayer were actually transferred onto the mica surface.

If one compares with Fig. 9A, the morphology of the LPS monolayer is dramatically changed upon insertion of the cationic plasticin: no LE/

Table 2
Structural parameters extracted from GIXD data of mixed LPS 3:1 monolayers alone or in the presence of 0.1 and 1 μM plasticins: momentum transfer in-plane $Q_{||}$ and out-of-plane Q_z components, corresponding d-spacings, primitive cell parameters a, b and γ(°), unit cell area A_0, in-plane and out-of-plane correlation lengths L_{xy} and L_z and area per LPS molecule A_{molec}.

System	Q_{xy} (Å^{-1})		Q_z (Å^{-1})		d-spacings (Å)		Primitive unit cell			Unit cell area A_0 (Å^2)	In-plane correlation length L_{xy} (Å)		Out-of-plane correlation length L_z (Å) *(10) peak*	Area per LPS molecule A_{molec} (Å^2)
	(10)	(01)	(10)	(01)	(10)	(01)	a (Å)	b (Å)	γ (°)		(10)	(01)		
Mixed LPS 3/1 alone	1.46	1.51	0.49	0.61	4.3	4.2	4.8	5.0	116	21.6	37	568	14	140.2
LPS 3/1 + PTCDA1 at 0.1 μM	1.36	1.51	0.51	0.61	4.6	4.2	4.6	5.0	113	21.2	30	238	14	140.6
LPS 3/1 + PTCDA1 at 1 μM	1.47	--	0.50	--	4.3	--	5.1	5.1	113	23.9	30	--	14	158.4
LPS 3/1 + PTCDA1-KF at 0.1 μM	No diffraction peak													
LPS 3/1 + PTCDA1-KF at 1 μM	No diffraction peak													

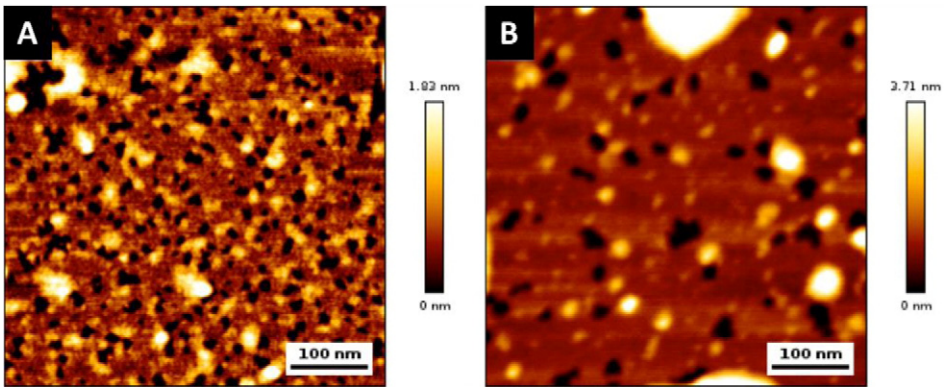

Fig. 9. AFM height images of the LB-transferred mixed LPS 3:1 monolayer before interaction (A), and after interaction with PTCDA1 at 1 μM (B). Images size: 500 nm, z-scales are shown on the right side of each picture. White patches are salt crystals.

LC domain organization is detected anymore, and the monolayer structure appears completely riddled with numerous small round-shaped aggregates of peptide, demonstrating the effective penetration of the cationic plasticin into the mixed LPS monolayer at 40 mN/m. The average thickness of the monolayer patch is around 8 nm (see inset in Fig. 10A). The aggregates protrude out from the monolayer with, in average, a height of 2 to 3 nm with respect to the surrounding monolayer, which makes a total height of 10–11 nm. Taking into account the convolution with the AFM tip radius, the aggregates are between 15 and 20 nm wide (see inset in Fig. 10B). This striking result confirms the ability of PTCDA1-KF to penetrate and disintegrate the mixed LPS monolayer. AFM also demonstrates that this peptide can insert and persist in the LPS monolayer in 20 nm in size aggregates, even at a surface pressure as high as 40 mN/m. These aggregates are very different from those that were imaged when PTCDA1-KF (1 μM) was LB-transferred on a mica surface after 50 min adsorption at the free buffer interface. Indeed, Fig. 10C shows donut-shaped objects. This particular shape is very probably due to the dehydration process that occurred after the LB transfer. The aggregates are 2.5 nm high in average and their spatial extension varies between 200 and 250 nm (Fig. 10D), which is one order of magnitude higher than the size of the small peptide aggregates embedded in the LPS monolayer (Fig. 10B). Knowing that these aggregates did not interact with LPS, this result confirms the disaggregation of the cationic plasticin before its insertion into the LPS leaflet.

4. Conclusion

Lipid monolayers and bilayers with different compositions have been used to model the OM of Gram negative bacteria: a mixture of smooth LPS/mutant LPS Re 595 was chosen for the external leaflet and ternary PL mixture for the inner one. We have focused on LPS monolayers mimicking the external leaflet to better understand the initial steps of peptide interaction with bacteria. Five parameters have been considered to be pertinent for the description of the interaction: the lipid nature of the mono- or bilayer, the charge, concentration, conformation and state of aggregation of the plasticins.

Our results constitute a first body of evidence to explain the difference in antibacterial activity between two plasticins PTCDA1 and PTCDA1-KF against Gram-negative bacteria. Peptide charge and aggregation patterns appear to be the relevant parameters that govern its

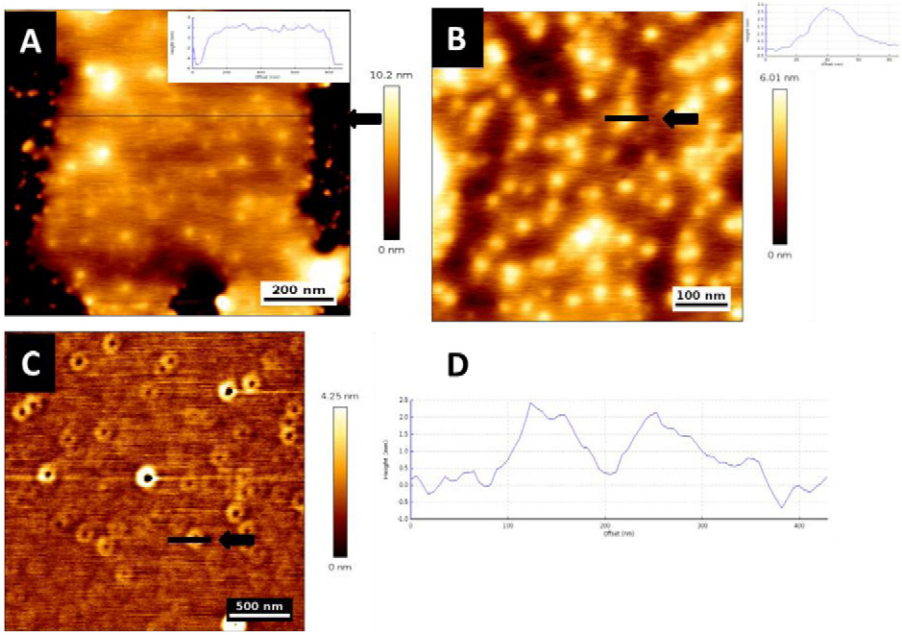

Fig. 10. (A and B) AFM height images (with 1 μm and 500 nm sizes) and associated height cross profiles as insets of the LB-transferred mixed LPS 3:1 monolayer after incubation with PTCDA1-KF at 1 μM. Image in B is a zoom made on image in A. (C) AFM height images (with 1.5 μm size) of the LB-transferred PTCDA1-KF at 1 μM, in the absence of LPS monolayer. (D) Height cross profile of the cationic plasticin aggregates performed along the line (black arrow) displayed in image in C and showing their donut-like shape in air.

conformation and ability to penetrate into the outer leaflet of the OM. The replacement of three amino acids in the peptide sequence, among which two of them are positively charged, provided a net positive charge to the modified plasticin. In interaction with anionic membranes only, PTCDA1-KF structured as oligomers of α-helices. The insertion and AFM experiments showed that the disaggregation that occurred upon interaction with bacterial lipids was a step necessary to enable its penetration as small oligomers of α-helices into the LPS matrix.

Based on these results, we are now able to establish the main features of the initial interaction of PTCDA1 and PTCDA1-KF with the bacterial OM.

a) At concentrations higher than the critical aggregation concentration, both plasticins aggregate in the aqueous subphase. The natural peptide forms large aggregates whereas for the cationic one, smaller oligomers of α helices coexist with large aggregates.
b) The kinetics of the interaction with the OM external leaflet is faster for the cationic plasticin.
c) Upon interaction with the polar face of the LPS leaflet, partial disaggregation occurs for the cationic plasticin, allowing the electrostatic adsorption of oligomers onto the polar face of the LPS leaflet. The natural plasticin remains aggregated upon interaction and unable to penetrate into the LPS monolayer.
d) Insertion of the cationic peptide takes place between the lipid molecules of the monolayer leading to higher surface pressure and molecular packing, and finally to the disorganization of the LPS monolayer. Further penetration into the internal leaflet of the OM is eased as the cationic peptide has already disaggregated upon its interaction with the LPS leaflet.

Acknowledgments

The authors acknowledge the financial support of University Paris Sud through their “Attractivité 2011” grant program, the Région Ile-de-France (“Equipement mi-lourd 2012” program, DIM Malinf) and the JPK Company for their active support. They are also grateful to C. El Amri and P. Joanne (UPMC) and Dr. S. Lesieur (UMR CNRS 8612, Institut Galien Paris Sud) for their fruitful discussions. They also thank SOLEIL synchrotron for providing beamtime on the SIRIUS beamline.

Appendix A. Supplementary data

Supplementary data to this article can be found online at http://dx.doi.org/10.1016/j.bbamem.2015.09.005.

References

[1] The bacterial challenge: time to react, ECDC Technical Report, 2009.
[2] G. Wang, X. Li, Z. Wang, APD2: the updated antimicrobial peptide database and its application in peptide design, Nucleic Acids Res. 37 (2009) D933–D937.
[3] Y. Shaï, Mode of action of membrane active antimicrobial peptides, Biopolymers 66 (4) (2002) 236–248.
[4] C. Lacombe, C. Cifuentes-Diaz, I. Dunia, M. Auber-Thomay, P. Nicolas, M. Amiche, Peptide secretion in the cutaneous glands of south American tree frog phyllomedusa bicolor: an ultrastructural study, Eur. J. Cell Biol. 79 (2000) 631–641.
[5] P. Nicolas, C. El Amri, The 39olymyxine39e superfamily: a gene-based combinatorial library of antimicrobial peptides, Biochim. Biophys. Acta 2009 (1788) 1537–1550.
[6] F. Bruston, C. Lacombe, K. Zimmermann, P. Nicolas, C. El Amri, Structural malleability of plasticins: preorganized conformations in solution and relevance for antimicrobial activity, Biopolymers 86 (2007) 46–52.
[7] C. El Amri, P. Nicolas, Plasticins: membrane-damaging peptides with ‘chameleon-like’ properties, Cell. Mol. Life Sci. 65 (2008) 895–909.
[8] C. Wechselberger, Cloning of cDNAs encoding new peptides of the dermaseptin-family, Biochim. Biophys. Acta 1388 (1998) 279–283.
[9] D. Vanhoye, F. Bruston, C. El Amri, A. Ladram, M. Amiche, P. Nicolas, Membrane association, electrostatic sequestration, and cytotoxicity of Gly-Leu-rich peptide orthologs with differing functions, Biochemistry 43 (26) (2004) 8391–8409.
[10] D. Vanhoye, F. Bruston, P. Nicolas, M. Amiche, Antimicrobial peptides from hylid and ranin frogs originated from a 150-million-year-old ancestral precursor with a conserved signal peptide but a hypermutable antimicrobial domain, Eur. J. Biochem. 270 (9) (2003) 2068–2081.
[11] C. El Amri, C. Lacombe, K. Zimmerman, A. Ladram, M. Amiche, P. Nicolas, F. Bruston, The plasticins: membrane adsorption, Lipid Disord. Biol. Act. Biochem. 45 (2006) 14285–14297.
[12] P. Joanne, M. Falord, O. Chesneau, C. Lacombe, S. Castano, B. Desbat, C. Auvynet, P. Nicolas, T. Msadek, C. El Amri, Comparative study of two plasticins: specificity, interfacial behavior, and bactericidal activity, Biochemistry 48 (2009) 9372–9383.
[13] P. Joanne, C. Galanth, N. Goasdoué, P. Nicolas, S. Sagan, S. Lavielle, G. Chassaing, C. El Amri, I. Alves, Lipid reorganization induced by membrane active peptides probed using differential scanning calorimetry, Biochim. Biophys. Acta Biomembr. 2009 (1772–1781) 1788.
[14] Y. Corvis, W. Barzyk, G. Brezesinski, N. Mrabet, M. Badis, S. Hecht, E. Rogalska, Interactions of a fungistatic antibiotic, griseofulvin, with phospholipid monolayers used as models of biological membranes, Langmuir 22 (2006) 7701–7711.
[15] A. Clausell, M. Garcia-Subirats, M. Pujol, M.A. Busquets, F. Rabanal, Y. Cajal, Gram-negative outer and inner membrane models: insertion of cyclic cationic lipopeptides, J. Phys. Chem. B 111 (3) (2007) 551–563.
[16] D. Gidalevitz, Y. Ishitsuk, A.S. Muresan, O. Konovalov, A.J. Waring, R.I. Lehrer, K.Y.C. Lee, Interaction of antimicrobial peptide protegrin with biomembranes, Proc. Natl. Acad. Sci. U. S. A. 100 (11) (2003) 6302–6307.
[17] F. Neville, Y. Ishitsuka, C.S. Hodges, O. Konovalov, A.J. Waring, R. Lehrer, K.Y.C. Lee, D. Gidalevitz, Protegrin interaction with lipid monolayers: grazing incidence X-ray diffraction and X-ray reflectivity study, Soft Matter 4 (2008) 1665–1674.
[18] K. Nomura, T. Inaba, K. Morigaki, K. Brandenburg, U. Seydel, S. Kusumoto, Interaction of lipopolysaccharide and phospholipid in mixed membranes: solid-state 31P-NMR spectroscopic and microscopic investigations, Biophys. J. 95 (3) (2008) 1226–1238.
[19] C. Merz, W. Knoll, M. Textor, E. Reimhult, Formation of supported bacterial lipid membrane mimics, Biointerphases 3 (2) (2008) FA41–FA50.
[20] C.M. Koppelman, T. Den Blaauwen, M.C. Duursma, R.M.A. Heeren, N. Nanning, Escherichia coli minicell membranes are enriched in cardiolipin, J. Bacteriol. 183 (20) (2001) 6144–6147.
[21] J.E. Cronan, Bacterial membrane lipids: where do we Stand? Annu. Rev. Microbiol. 57 (2003) 203–224.
[22] D.E. Graham, M.C. Phillips, Kinetics of adsorption and surface denaturation, J. Colloid Interface Sci. 70 (1979) 403–414.
[23] P. Suttiprasit, V. Krisdhasima, J. McGuire, The surface activity of α-lactalbumin, β-lactoglobulin, and bovine serum albumin, J. Colloid Interface Sci. 154 (1992) 316–326.
[24] J.T. Davies, E.K. Rideal, Interfacial Phenomena, 2nd ed. Academic Press, New York, 1963 265.
[25] P. Calvez, E. Demers, E. Boisselier, C. Salesse, Analysis of the contribution of saturated and polyunsaturated phospholipid monolayers to the binding of proteins, Langmuir 27 (4) (2011) 1373–1379.
[26] E. Boisselier, P. Calvez, E. Demers, L. Cantin, C. Salesse, Influence of the physical state of phospholipid monolayers on protein binding, Langmuir 28 (2012) 9680–9688.
[27] A.D. Bangham, M.M. Standish, J.C. Watkins, Diffusion of univalent ions across the lamellae of swollen phospholipids, J. Mol. Biol. 13 (1965) 238.
[28] V. Faivre, V. Rosilio, P. Boullanger, L. Martins Almeida, A. Baszkin, Fucosyled neoglycolipids: synthesis and interaction with a phospholipid, Chem. Phys. Lipids 109 (2001) 91.
[29] G. D'Errico, A. Silipo, G. Mangiapia, A. Molinaro, L. Paduano, R. Lanzetta, Mesoscopic and microstructural characterization of liposomes formed by the lipooligosaccharide from *Salmonella* Polymyxin strain 595 (Re-mutant), Phys. Chem. Chem. Phys. 11 (2009) 2314.
[30] http://dichroweb.cryst.bbk.ac.uk
[31] http://bioinformatik.biochemtech.uni-halle.de/cdnn/
[32] P. Fontaine, G. Ciatto, N. Aubert, M. Goldmann, Soft interfaces and resonant investigation on undulator source: a surface X-ray scattering beamline to study organic molecular films at the SOLEIL synchrotron, Sci. Adv. Mater. 6 (2014) 2312–2316.
[33] A. Blume, A comparative study of the phase transitions of phospholipid bilayers and monolayers, Biochim. Biophys. Acta 557 (1979) 32–44.
[34] A. Guinier, X.-R. Diffraction, Freeman, San Francisco, Chap. 5 (1968) 1.
[35] F. Bruston, C. Lacombe, K. Zimmermann, C. Piesse, P. Nicolas, C. El Amri, Structural malleability of plasticins: preorganized conformations in solution and relevance for antimicrobial activity, Biopolymers 86 (2007) 42–56.
[36] K. Brandenburg, U. Seydel, Investigation into the fluidity of lipopolysaccharide and free lipid a membrane systems by Fourier-transform infrared spectroscopy and differential scanning calorimetry, Eur. J. Biochem. 191 (1990) 229–236.
[37] S. Roes, U. Seydel, T. Gutsmann, Probing the properties of lipopolysaccharide monolayers and their interaction with the antimicrobial peptide Polymyxine B by atomic force microscopy, Langmuir 21 (2005) 6970–6978.
[38] J. Minones Jr., J.M. Rodrıguez-Patino, O. Conde, C. Carrera, R. Seoane, The effect of polar groups on structural characteristics of phospholipid monolayers spread at the air–water interface, Colloids Surf. A. 203 (2002) 273–286.
[39] C. Jeworrek, F. Evers, J. Howe, K. Brandenburg, M. Tolan, R. Winter, Effects of specific versus nonspecific ionic interactions on the structure and lateral organization of lipopolysaccharides, Biophys. J. 100 (2011) 2169–2177.
[40] M. Zasloff, Magainins, a class of antimicrobial peptides from xenopus skin: isolation, characterization of two active forms, and partial cDNA sequence of a precursor, Proc. Natl. Acad. Sci. U. S. A. 84 (1987) 5449–5453.